MAPPING 3-D STRUCTURE USING 2-D SEISMIC

Richard T. Houck, Nancy J. House-Finch, Dan G. Carpenter, Marvin L. Johnson

Mobil, Dallas

Published in the August 1996 issue of The Leading Edge

Everyone who's tried to make a structure map from a 2-D seismic grid knows that you can't *uniquely* map a 3-D structure with 2-D seismic. Even if you were perfectly accurate in picking reflection times and converting the times to depth, there would still be many possible reflecting surfaces that could have produced the same set of 2-D picks. This non-uniqueness is commonly treated purely as a sampling issue - you don't have any coverage between the lines, so you are free to contour these regions in any geologically reasonable way.

In fact, the situation is more complicated than this. Because 2-D migration operates only in the inline direction, the crossline locations of the reflection points are unknown (Whitcombe and Carroll, Geophysics 1994 v. 59, p. 1121-1132). This incomplete migration causes the misties that are typically observed on 2-D grids. Procedures such as map migration and trackline construction try to correct for the incompleteness of 2-D imaging. However, these methods assume that any crossline structure is smooth enough to be adequately represented by interpolating the 2-D grid, and are often unusable for complex or deep structures. So, not only does 2-D seismic result in a non-uniform distribution of reflection points, you don't know the crossline locations of the reflection points you do have.

Although a grid of 2-D picks can't uniquely determine a 3-D structure, it *can* be used to impose specific constraints on which 3-D structures are possible. Using these constraints, we can produce a whole range of possible 3-D structures, all of which are consistent with the 2-D interpretation. One of these maps is the right structure, but the 2-D grid is incapable of determining which one it is. The variability in this set of structure maps is a measure of the structural uncertainty inherent in the 2-D grid. This uncertainty is due entirely to the incompleteness of 2-D imaging, and would not be present in 3-D seismic. Eliminating this structural uncertainty is one of the main motivations for using 3-D seismic.

The usual approach to 2-D mapping treats the picks made on 2-D migrations as point values of time or depth structure that can be mapped directly. However, the real structure almost certainly violates the assumptions behind 2-D imaging, resulting in misties that may be valid picks but are unmappable using conventional methods. A more realistic approach is to treat the 2-D picks as *indirect observations* that constrain the possible structures, instead of as structure to be mapped. The next section describes how a grid of 2-D picks can be used to generate a surface that constrains the possible 3-D structures.

STRUCTURAL CONSTRAINTS

As shown in Figure 1a, reflection points are commonly mapped vertically in the plane of the seismic line, but their true locations may be anywhere on a curve that extends in the crossline direction. This curve corresponds to crossline section through a wavefront. For constant velocity media, the curves are circles; for arbitrary V(z), the curves are Kirchhoff time migration operators. But, as shown in Figure 1b, some of the possible locations may be ruled out by picks from nearby lines. For example, the conventional mapping of the pick on Line 1 (vertically below the shot point) is ruled out by the deep pick made on Line 2. If the reflector really were vertically below Line 1, an arrival would have been observed on Line 2 earlier than the one actually picked. If the pick on Line 2 is correct, the pick on Line 1 *must* be from out of the plane.

Keeping the deepest curve at every location where more than one curve exists defines a surface that constrains the possible reflecting surfaces (Figure 1c). Whatever the true reflecting surface is, it must touch the constraint surface at enough points to explain the observed reflections. Elsewhere, the reflector can vary freely, but it can *never* be shallower than the constraint surface. Figures 1d and 1e are examples of two reflecting surfaces that satisfy these conditions.

The procedure outlined in Figure 1 is based on two assumptions. First, all reflection points are assumed to have been correctly positioned inline by performing a valid 2-D time migration. Second, all picks are assumed to be post-migration first arrivals from a single, but not necessarily continuous, reflector. Essentially, these assumptions say that the constraint surface will be correct if the processing is correct and the picks are correct. In the case of a faulted reflector, the "first arrival" assumption means that a diffracted arrival from the upthrown side of a fault should be picked if it arrives before a specular reflection from the downthrown side.

Generating the constraint surface can be viewed as a partial application of the old "wavefront chart" migration method described by Musgrave (Q. Colo. Sch. Mines 1952 v.47, no. 4). This method involves moving reflection picks along the same curves depicted in Figure 1, but operates in the inline direction instead of crossline. Because the picks are being migrated inline, an estimate of the time dip can be used to determine exactly where along the wavefront curve each reflection point should go. In our case, sparse crossline sampling makes it difficult to get a reliable estimate of time dip. If the crossline structure were sufficiently smooth, we could fit a smooth curve to the picks and get the required time dips from the interpolated reflector. This is essentially the approach used in map migration. If the crossline structure cannot be assumed to be smooth, the best we can do is to eliminate the loose ends of the wavefront curves as shown in Figure 1c. Then, instead of definite reflection point locations for each pick, we have a range of possible locations, determined by the constraint surface.

Figure 1 shows how a set of 2-D migrated picks generates a surface that constrains the possible 3-D structures. Next, we show how this procedure can be applied to an interpreted 2-D grid.

OVERTHRUST EXAMPLE

The map in Figure 2 shows an interpreted 2-D grid from an overthrust area in the U.S. Time picks were made from time migrated sections and converted to depth. Picks are posted at the surface locations of their shot points; misties have not been resolved. Figure 3 shows the conventional 2-D map made from the posted picks. The target structure is the high near the center of the map. Before contouring the structure in Figure 3, misties between the picks in Figure 2 were resolved using a procedure similar to trackline construction.

Standard practice would be to use the map in Figure 3 to estimate the volume of the trapping structure as if there were no uncertainty in the geometry of the trap. But, Figure 3 is *not* the only possible reflecting surface that could have produced the picks in Figure 2. Despite the fact that misties have been resolved, it's possible (likely) that the mapped reflector *conflicts* with some of the observed picks. Modeling zero offset sections along the 2-D lines and migrating the resulting "stacks" would not necessarily produce the same set of picks shown in Figure 2. Not only is the map in Figure 3 not the only possible structure, it may not even be an allowed structure.

To find all possible reflecting surfaces that are consistent with the observed picks, we have to define how the set of 2-D picks in Figure 2 constrains the underlying 3-D structure. Figure 4 shows the constraint surface produced by sweeping each pick over all its possible crossline locations and keeping the deepest value at each map point as in Figure 1. Depth picks have been treated as if they were time picks from a constant velocity medium, and have been swept out along circular curves. A more accurate approach would have been to use the original time picks, and sweep them out along migration operators using the velocity model. The error incurred by using depths directly is equivalent to performing Kirchhoff time migration using average velocity instead of RMS velocity.

A useful analogy is to view the constraint surface in Figure 4 as being like a blanket thrown over the real structure. The true structure touches this surface at some points, is below it at others, but never goes above it. The blanket analogy explains why smooth structures mapped from 2-D seismic often turn out to be broken up when 3-D seismic becomes available. Although there may be a smooth structure (similar to the map in Figure 3) that fits under the constraint surface, there are numerous broken structures that are equally consistent with the 2-D interpretation.

By keeping track of which parts of the constraint surface are associated with each seismic line, we can identify all the possible locations for reflection points from that line. Figure 5 shows the swath of possible reflection points for line W-8. In some places, such as at the northwest end of the line, *all* of the original reflection point locations are possible, including the conventional mapping vertically below the shotpoint. In other locations, the reflection points are *required* to be out of the plane. This is the situation illustrated in Line 1 of Figure 1b. Finally, because this is a real data set, there are gaps in the reflection point swath that indicate "inconsistent picks". The picks in these intervals are too high relative to nearby lines for *any* of the possible reflection point locations to be allowed. Inconsistent picks are caused by errors either in picking or in depth conversion, although the error isn't necessarily in the line that has the gap.

Identifying picks as "inconsistent" or "out of the plane" is based entirely on comparison with picks from nearby lines. Typically, there is no indication on the 2-D section that there is anything unusual in these zones. Figure 6. shows the interpreted section for Line W-8, corresponding to the reflection point swath in

Figure 5. The mapped horizon is indicated in orange. Neither the "out-of-the-plane" zone or the "inconsistent picks" zone is easily distinguishable from any other part of the reflector. In fact, it's possible that *all* of the reflection points are really out of the plane. The zone identified as out-of-the-plane on the swath just happens to have enough nearby coverage to force the reflection points to be mapped out of the plane.

A reflection point swath like the one in Figure 5 can be extracted from the constraint surface for every line in the 2-D grid. *Any* selection of reflection points from a reflection point swath is a valid mapping of the picks for that line. Selecting reflection points from the swaths automatically resolves the misties that occur between 2-D migrations over 3-D structures. One of the conflicting points will either be forced out of the plane, or will be identified as "inconsistent" if there are no allowable out-of-the-plane mappings.

This example has illustrated a general procedure for generating a map of a 3-D structure from 2-D seismic. First, select a set of reflection points from the swath for each line. Then, contour between the reflection points without going above the constraint surface. Forward modeling using any map made this way is *guaranteed* to reproduce the picks from the original interpretation.

By incorporating these steps into an automated mapping procedure, we can generate large numbers of structure maps that are all consistent with the original interpretation. The variability in these maps is a measure of the structural uncertainty in the 2-D grid. One way we can use this set of structure maps is to quantify the contribution of 2-D imaging to the uncertainty in trap volume.

UNCERTAINTY IN GROSS ROCK VOLUME

Uncertainty in the mapped structure is a major factor affecting estimates of hydrocarbon volumes. Wolf and Logel (1991 SEG Abstracts), and Hwang and McCorkindale (TLE, April 1994) describe how geostatistical conditional simulation can be used to assess the effect of velocity uncertainty on structure maps. Stoessel (TLE, April 1994) includes picking errors to get maps of combined depth uncertainty. For structures mapped from 2-D seismic, the inherent mapping indeterminacy described above adds to these two effects.

Volumes estimated from conventional 2-D maps not only fail to account for mapping non-uniqueness, but also tend towards overestimation because of mis-mapped out-of-the-plane reflections. Figure 7 shows how crossline dip tends to broaden structural highs. For isolated structures, this effect results in overestimated volumes.

Because it forces some reflection points to be mapped out of the plane of the 2-D line, the procedure described here removes some (but not all) of the overestimation bias illustrated in Figure 7. We can't remove *all* of the overestimation bias because we don't know where the reflection points really are. Selecting reflection points from the constraint surface guarantees that the selections are consistent with the seismic picks, but does not guarantee that the selections are the true reflection points.

We will estimate volume uncertainty by generating a set of possible structure maps and computing a trap volume for each map. The collection of volumes can then be used to construct a cumulative distribution function for gross rock volume. The resulting volume distribution will reflect the uncertainty due to the 2-D nature of the seismic grid. Uncertainties that are not specific to 2-D seismic, including uncertainties associated with picking or depth conversion, will *not* be reflected in the volume distribution.

Structure maps will be generated by selecting from the reflection point swaths the deepest allowed reflection point at each shot point. Geostatistical simulation (modified to include the constraint surface) is then used to define structural depths between the reflection points. Because all structure maps are generated from a single set of reflection points, this approach underestimates the true structural variability in the 2-D grid. This particular choice of reflection points is the closest to conventional 2-D mapping, and has the advantage of always producing a geologically reasonable set or reflection points without manual intervention.

Figure 8 shows the results of applying the volume uncertainty procedure to the overthrust example. The plotted volumes are for the high in the center of the map. Each point on the plot represents a simulated structure map; examples of two of the maps are shown in the Figure. Gross rock volumes have been computed assuming three different depths for the gas-water contact. The three contact depths are indicated by the three different plot symbols. Based on an externally specified uncertainty in contact depth, volume distributions from the three contact levels are combined to get a final volume distribution.

The quantity on the X-axis of Figure 8 is a geostatistical parameter that controls the smoothness of the structure - the higher this value, the smoother the structure. Different values of this parameter specify different covariance models. In most geostatistical applications, a covariance model would be estimated from the data. In our case, however, the data values (depth converted 2-D migrated times) are not simply related to structural depth (the quantity we are simulating). So, instead of trying to estimate covariance, we have run simulations for a *range* of covariances. Volumes from all the covariance models will be combined in our final distribution.

As expected, trap volume increases as the structure becomes smoother. Eventually, however, the structure can't be made larger without conflicting with the observed seismic. There is no inherent *lower* limit to structural size. In principle, the observed seismic picks could have resulted from a particular spatial distribution of point scatterers, with no associated trap volume. In practice, a lower limit for structural smoothness is set based on the geologic plausibility of the resulting structure maps.

Figure 9 shows cumulative distribution functions (dashed blue lines) constructed for each contact depth using the computed volumes. Cdf's for each contact depth are combined to get an overall cdf for the structure (red line). When computing the cdf's, volumes may be combined using externally assigned weights. In this example, volumes for each covariance model have been weighted using values that are approximately log normal in "nominal area" (covariance length2).

The black dashed line in Figure 9 is the volume estimate made from the conventional 2-D map in Figure 3, using a 3000m contact depth. The conventional volume is about 85% of the maximum volume on the simulated cdf for this contact (the center blue curve). This means that 85% of the possible structures had smaller volumes than the single structure map that would have been used for a conventional volume estimate.

Experiments with synthetic data, where the true volume is known, have shown that this procedure significantly reduces overestimation bias. For a model with similar complexity, a 40% volume overestimation by conventional methods was reduced to a 12% overestimation.

Summary and Conclusions. Because of irregular spatial sampling and unknown reflection point locations, there are many possible 3-D structures that can explain an interpreted 2-D seismic grid. Although they can't be mapped directly, a set of 2-D picks *can* be used to generate a surface that constrains the possible structures. The constraint surface can be used to produce an ensemble of structure maps that *all* reproduce the original picks. The variability in these maps is a measure of the structural uncertainty characteristic of the 2-D grid.

The volumetrics example described in this paper is one of several possible applications for the structural constraint surface. Other applications include manual mapping and acquisition planning. A manual version of the automated mapping method used for volumetrics would enable the interpreter to resolve misties and produce a contoured surface that is guaranteed to reproduce the original picks.

Depending on the geometry of the underlying structure and the layout of the 2-D grid, it may be possible to produce distinct, geologically realistic structure maps with significantly different prospectivities. In such cases, additional seismic would be needed to distinguish among the competing structure maps. Proposed infill line locations could be tested by forward modeling the new 2-D grid over the candidate structures, then generating new constraint surfaces for each set of modeled picks. If the infilled grid does not result in significantly different constraint surfaces for the competing structures, that particular layout provides no new structural information.

The constraint surface provides a robust method for producing data-consistent maps of 3-D structures using 2-D seismic. It does *not* provide a substitute for true 3-D seismic. However, by making it possible to estimate the structural uncertainty associated with a 2-D grid, it gives the geophysicist an objective way of separating cases where 2-D seismic can provide adequate structural information from cases where 3-D seismic is required.

REFERENCES.

Hwang, L., and McCorkindale, D., 1994, Troll field depth conversion using geostatistically derived average velocities: The Leading Edge, 13, 262-269.

Musgrave, A.W., 1952, Wavefront charts and raypath plotters, Q. Colo. Sch. Mines, v 47, no. 4.

Stoessel, E.T., 1994, The alliance between uncertainty and credibility: The Leading Edge, 13, 270-272.

Whitcombe, D.N. and Carroll R.J., 1994, The application of map migration to 2-D migrated data: Geophysics, 59, 1121-1132.

Wolf, D.J. and Logel, J.D., 1991, Geostatistics and depth conversion in the southern North Sea Basin: SEG Expanded Abstracts.

LIST OF FIGURES

Figure 1. Structural Non-Uniqueness in 2-D Seismic. 2-D migration can properly position reflection points inline, but their crossline locations are unknown. This sequence of crossline sections illustrates the implications of this incomplete imaging when the true reflecting surface is 3-D. (a) Reflection points are normally mapped in the plane of the seismic line, but their true locations could be anywhere on a curve extending in the crossline direction. (b) Picks from nearby lines may rule out some of the possible locations. If the pick on Line 2 is correct, the pick on Line 1 must have come from out of the plane. (c) Eliminating the parts of the curves that have been ruled out produces a surface that constrains the possible structures. The true reflecting surface must touch the constraint surface at enough points to explain the observed picks, and can never be shallower than the constraint surface. Any reflector that satisfies these conditions could have produced the observed picks; (d) and (e) are two of many such reflectors.

Figure 2. Interpreted 2-D Grid. Picks from a 2-D grid in an overthrust area in the U.S. have been converted to depth and posted at their shotopint locations.

Figure 3. Conventional 2-D Structure Map. This is the result of contouring the picks in Figure 2 in the conventional manner; the target structure is the high in the center of the map. However, this is not the only possible reflecting surface that could have produced these picks.

Figure 4. Structural Constraint Surface. This surface was generated by applying the procedure in Figure 1 to the picks in Figure 2. The true structure touches this surface at some points, but can never go above it.

Figure 5. Reflection Point Swath for Line W-8. The part of the constraint surface associated with each seismic line defines all the possible reflection point locations for that line. Certain intervals may be identified as being inconsistent with surrounding picks, or as originating out of the plane. Any selection of reflection points from this swath is a valid mapping of the reflection points for this line.

Figure 6. Line W-8 Migration. Zones identified in the reflection point swath as "inconsistent" or "out-of-the-plane" do not appear to be anomalous on the seismic section.

Figure 7. Structure Broadening from Crossline Dip. By mis-positioning out-of-the-plane reflections, conventional 2-D mapping makes structural highs appear to be broader than they really are. For an isolated high, this results in overestimating the volume of the structural trap.

Figure 8. Estimating Uncertainty in Gross Rock Volume. Geostatistical simulation, modified to include the constraint surface, has been used to generate a set of possible structure maps for the picks in Figure 2. Computing the gross rock volume for each map provides a measure of the volume uncertainty inherent in the 2-D grid. The scatter plot displays gross rock volume as a function of structural smoothness. The three plot symbols indicate three assumed contact depths. Each point on the plot corresponds to a structure map; three of the maps are shown in the Figure. Volume increases as the structure becomes smoother, but the seismic data imposes an upper limit on volume.

Figure 9. Cumulative Distribution Function for Gross Rock Volume. The three dashed blue lines ar the cdf's for each of the three assumed contact depths. The solid red line is the combined cdf for all contacts. The conventional volume estimate for the 3000m contact (dashed black line) was calculated from the map in Figure 3. The conventional estimate is higher than about 85% of the simulated volumes for the same contact depth.

FIGURE 1

Crossline Section Through Three 2-D Migrated Lines

lines extend out of the page

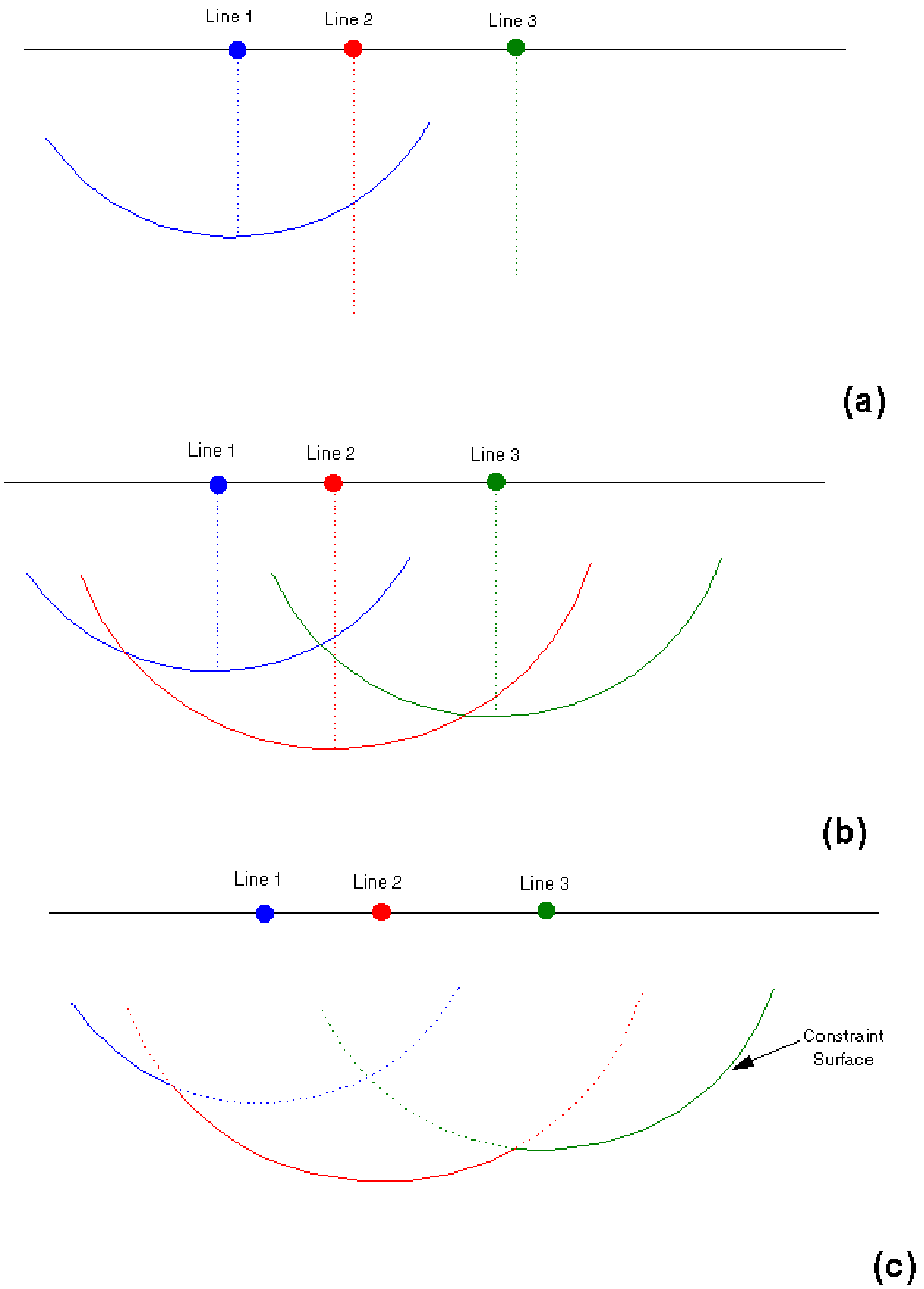

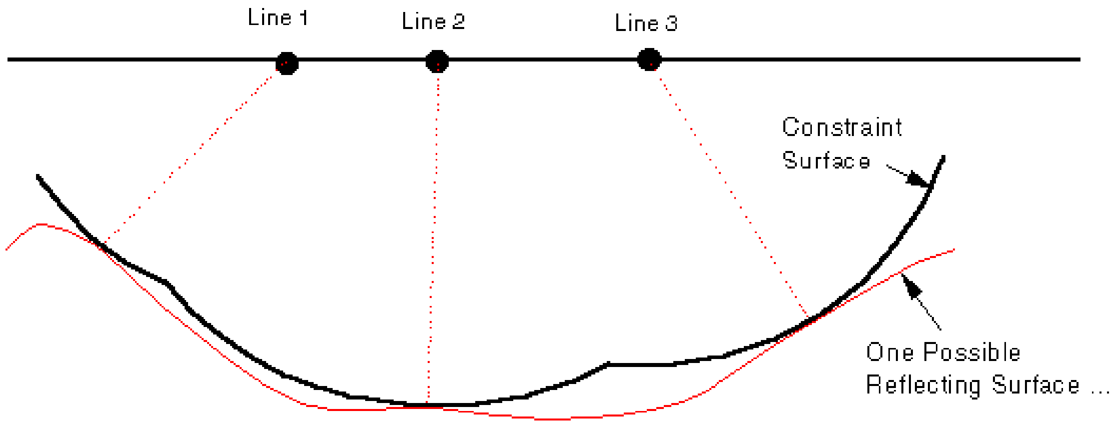
Line 1
Line 2
Line 3
Constraint
Surface
One Possible
Reflecting Surface ...

(d)

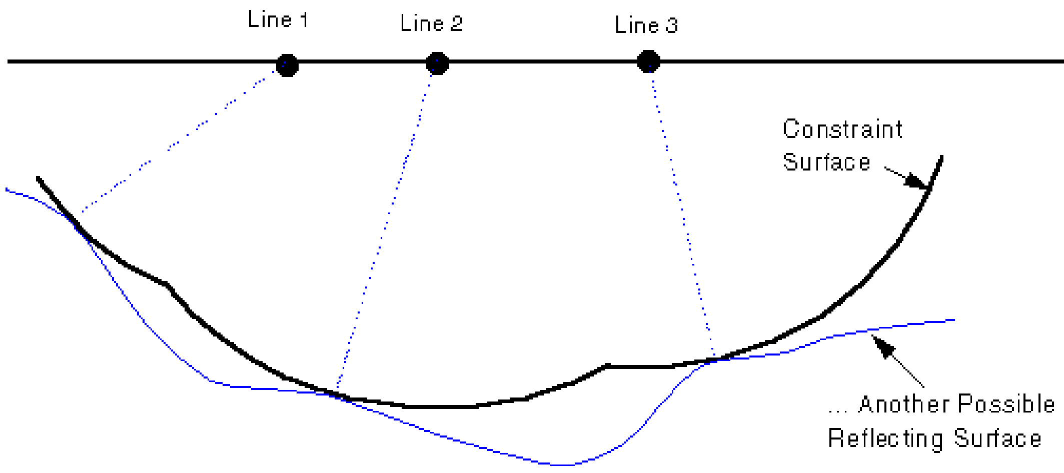
Line 1
Line 2
Line 3
Constraint
Surface
... Another Possible
Reflecting Surface

(e)

FIGURE 2

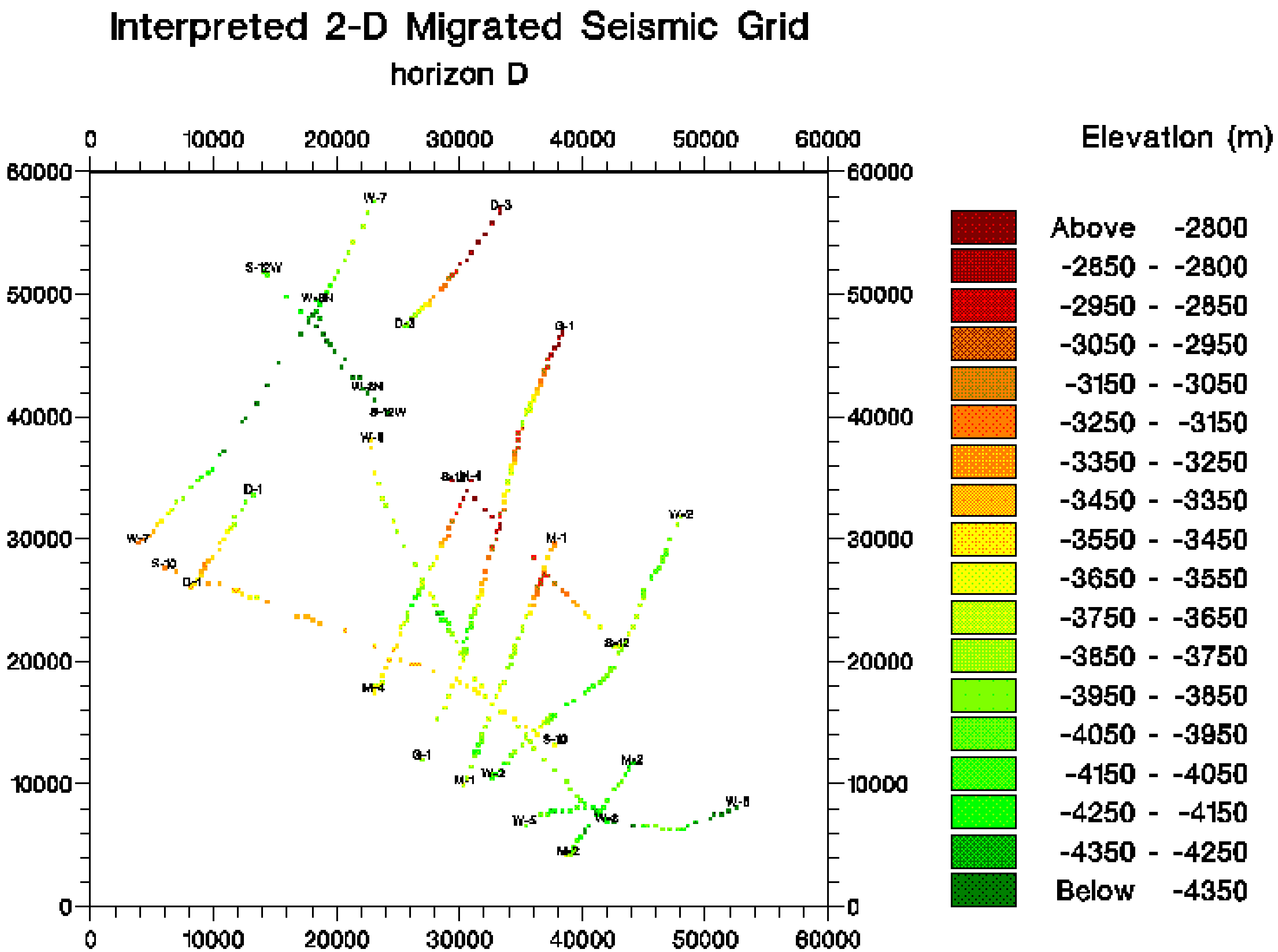
Interpreted 2-D Migrated Seismic Grid
horizon D
Elevation (m)
Above -2800
-2850 - -2800
-2950 - -2850
-3050 - -2950
-3150 - -3050
-3250 - -3150
-3350 - -3250
-3450 - -3350
-3550 - -3450
-3650 - -3550
-3750 - -3650
-3850 - -3750
-3950 - -3850
-4050 - -3950
-4150 - -4050
-4250 - -4150
-4350 - -4250
Below -4350

FIGURE 3

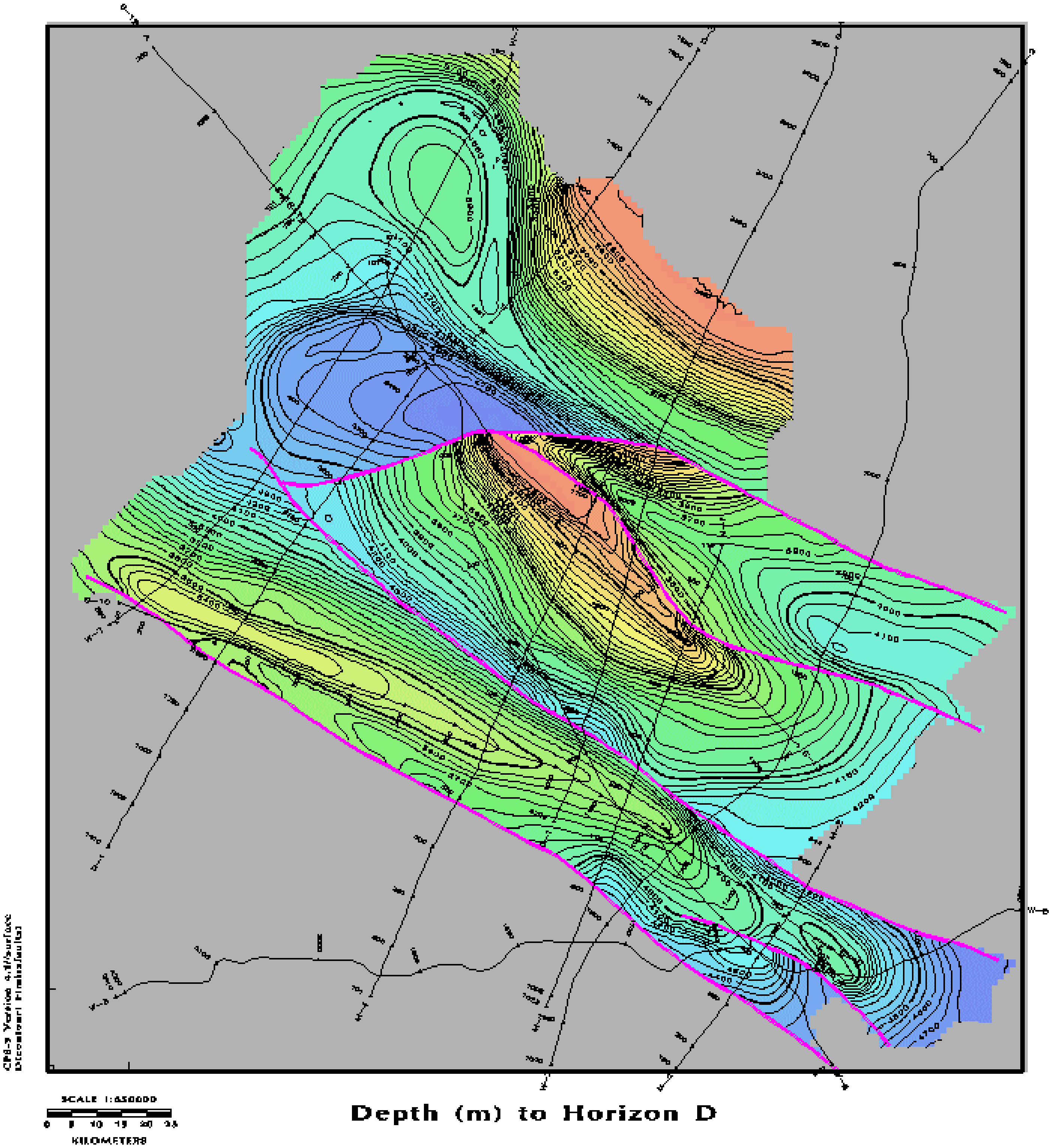

Depth (m) to Horizon D

FIGURE 4

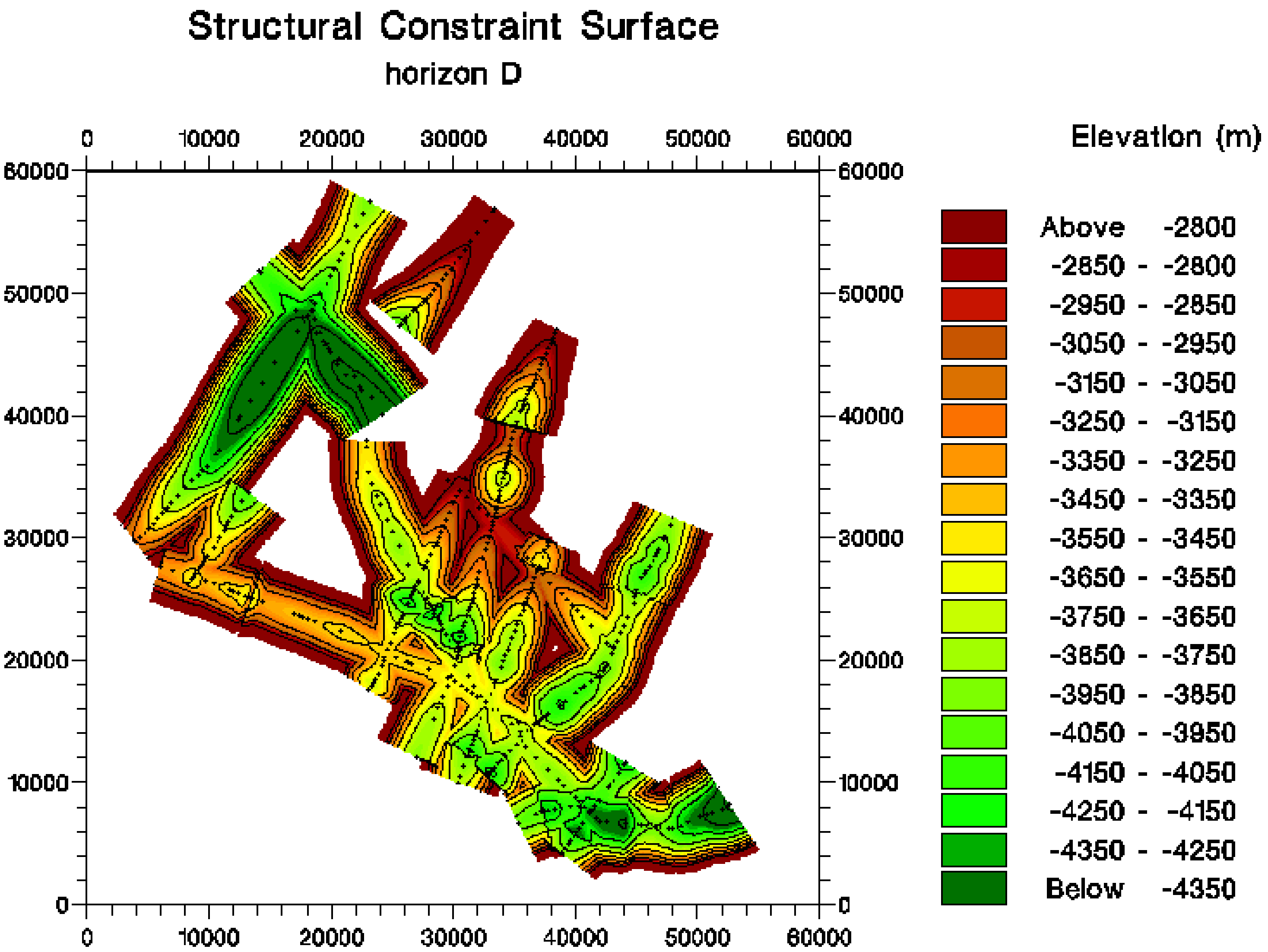
Structural Constraint Surface
horizon D
Elevation (m)
Above -2800
-2850 - -2800
-2950 - -2850
-3050 - -2950
-3150 - -3050
-3250 - -3150
-3350 - -3250
-3450 - -3350
-3550 - -3450
-3650 - -3550
-3750 - -3650
-3850 - -3750
-3950 - -3850
-4050 - -3950
-4150 - -4050
-4250 - -4150
-4350 - -4250
Below -4350
0
10000
20000
30000
40000
50000
60000

FIGURE 5

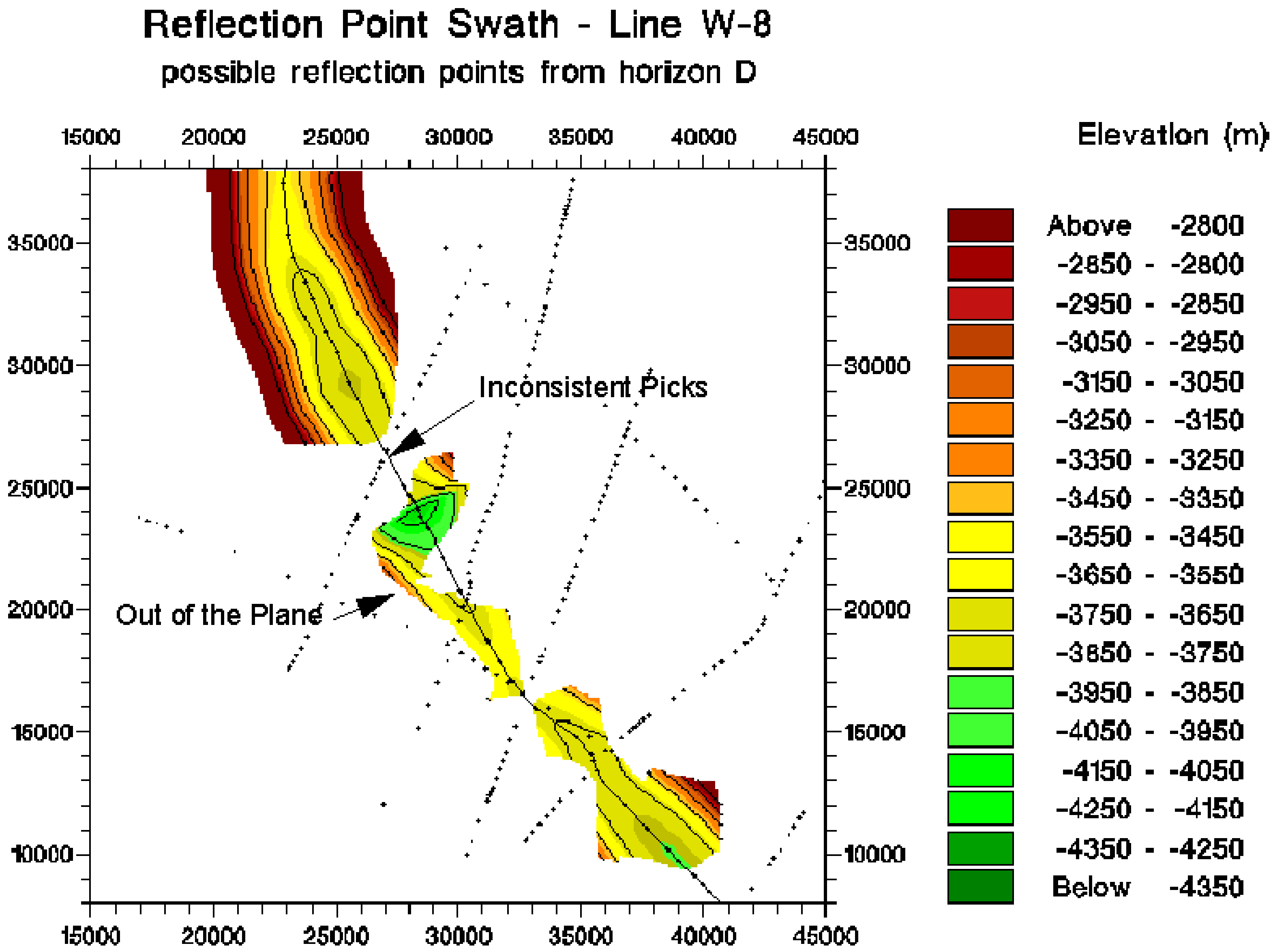
Reflection Point Swath - Line W-8
possible reflection points from horizon D
15000
20000
25000
30000
35000
40000
45000
10000
Inconsistent Picks
Out of the Plane
Elevation (m)
Above -2800
-2850 - -2800
-2950 - -2850
-3050 - -2950
-3150 - -3050
-3250 - -3150
-3350 - -3250
-3450 - -3350
-3550 - -3450
-3650 - -3550
-3750 - -3650
-3850 - -3750
-3950 - -3850
-4050 - -3950
-4150 - -4050
-4250 - -4150
-4350 - -4250
Below -4350

FIGURE 6

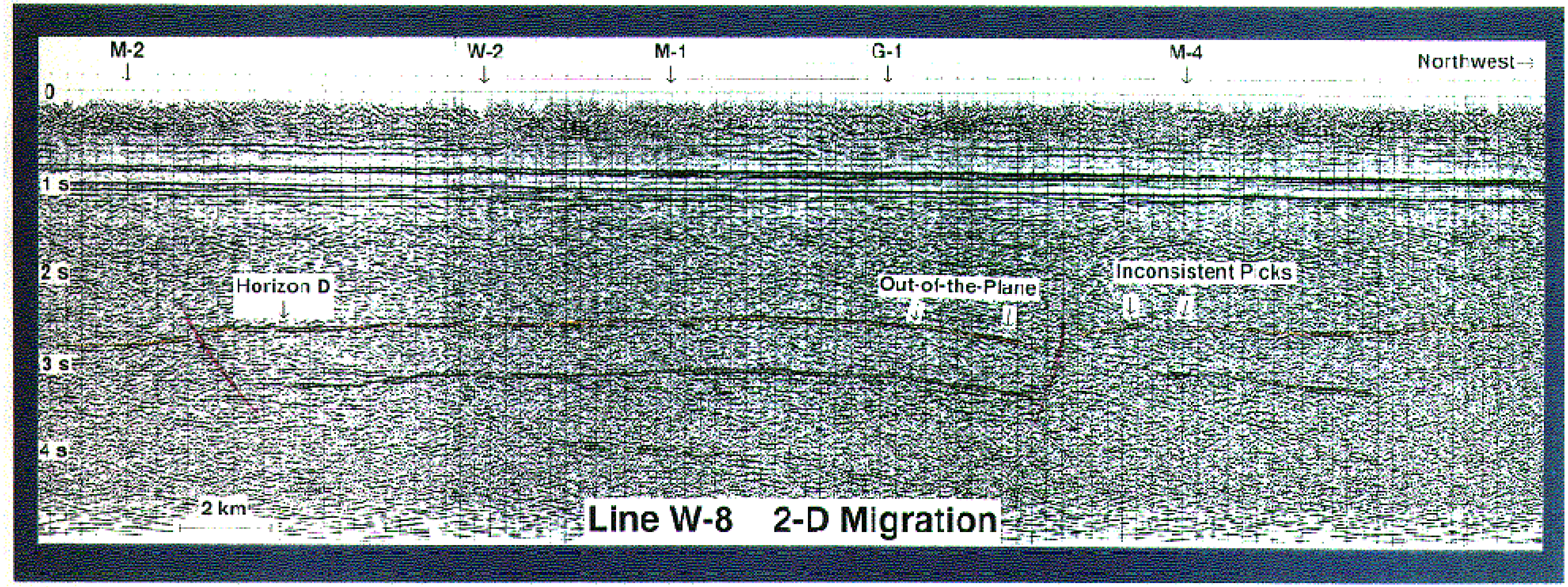
M-2
W-2
M-1
G-1
M-4
Northwest→
0
1 s
2 s
3 s
4 s
Horizon D
Out-of-the-Plane
Inconsistent Picks
2 km
Line W-8 2-D Migration

FIGURE 7

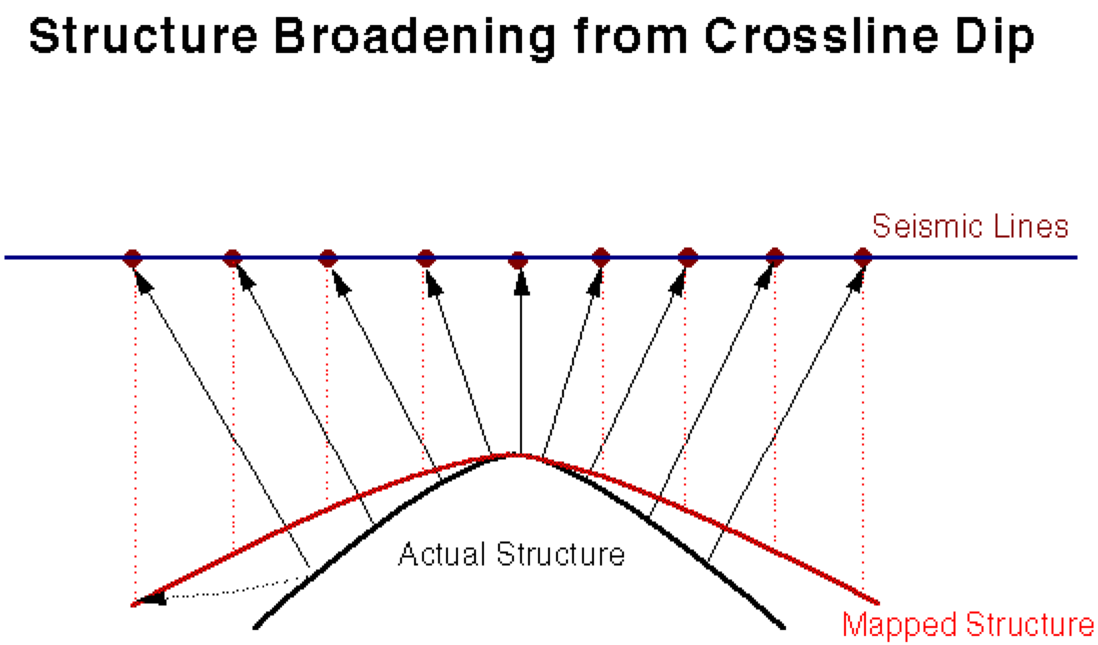
Structure Broadening from Crossline Dip
Seismic Lines
Actual Structure
Mapped Structure

FIGURE 8

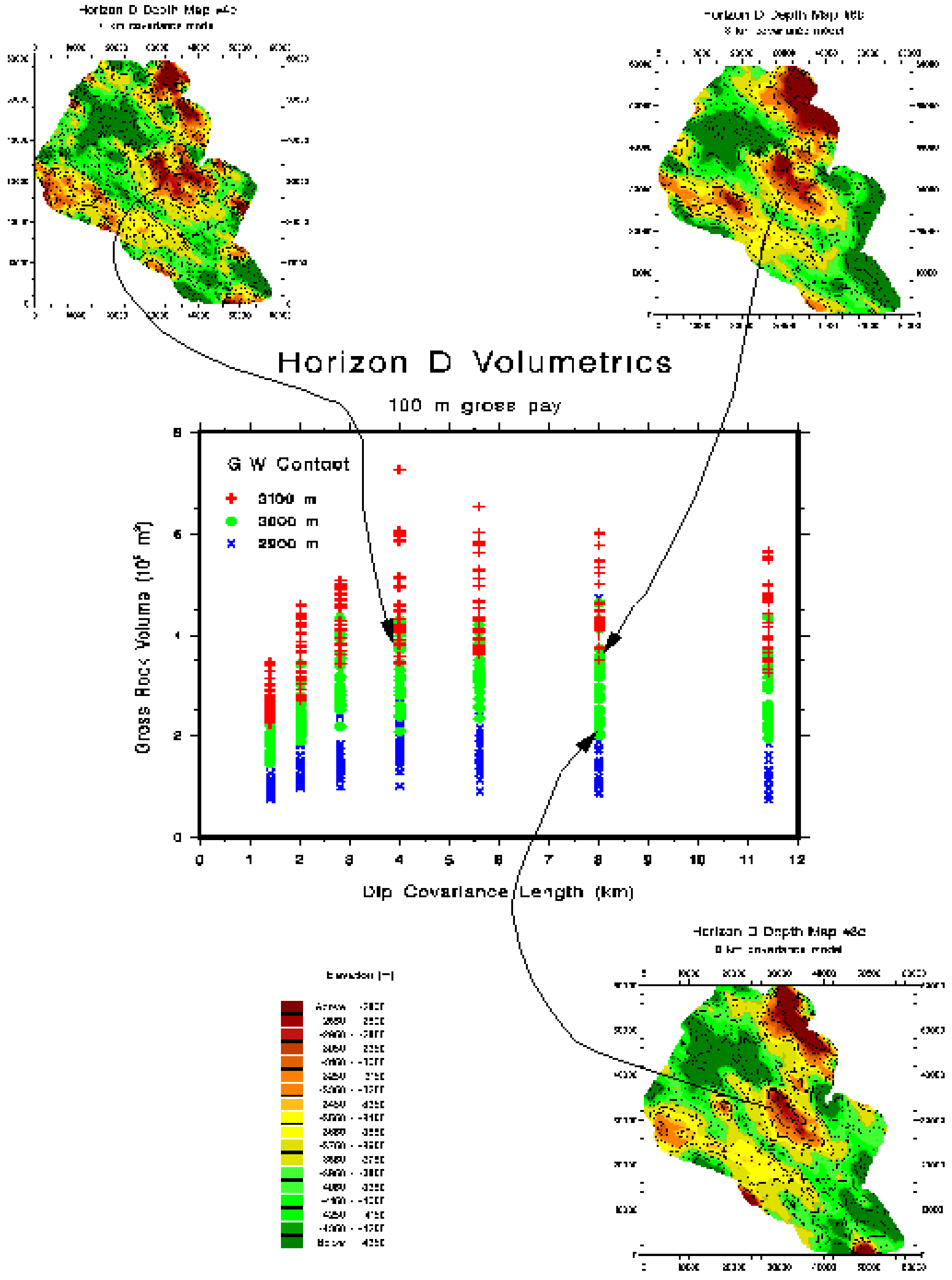
Horizon D Volumetrics
100 m gross pay
G W Contact
3100 m
3000 m
2900 m
Gross Rock Volume (10^6 m^3)
0
2
4
6
8
0 1 2 3 4 5 6 7 8 9 10 11 12
Dip Covariance Length (km)

FIGURE 9

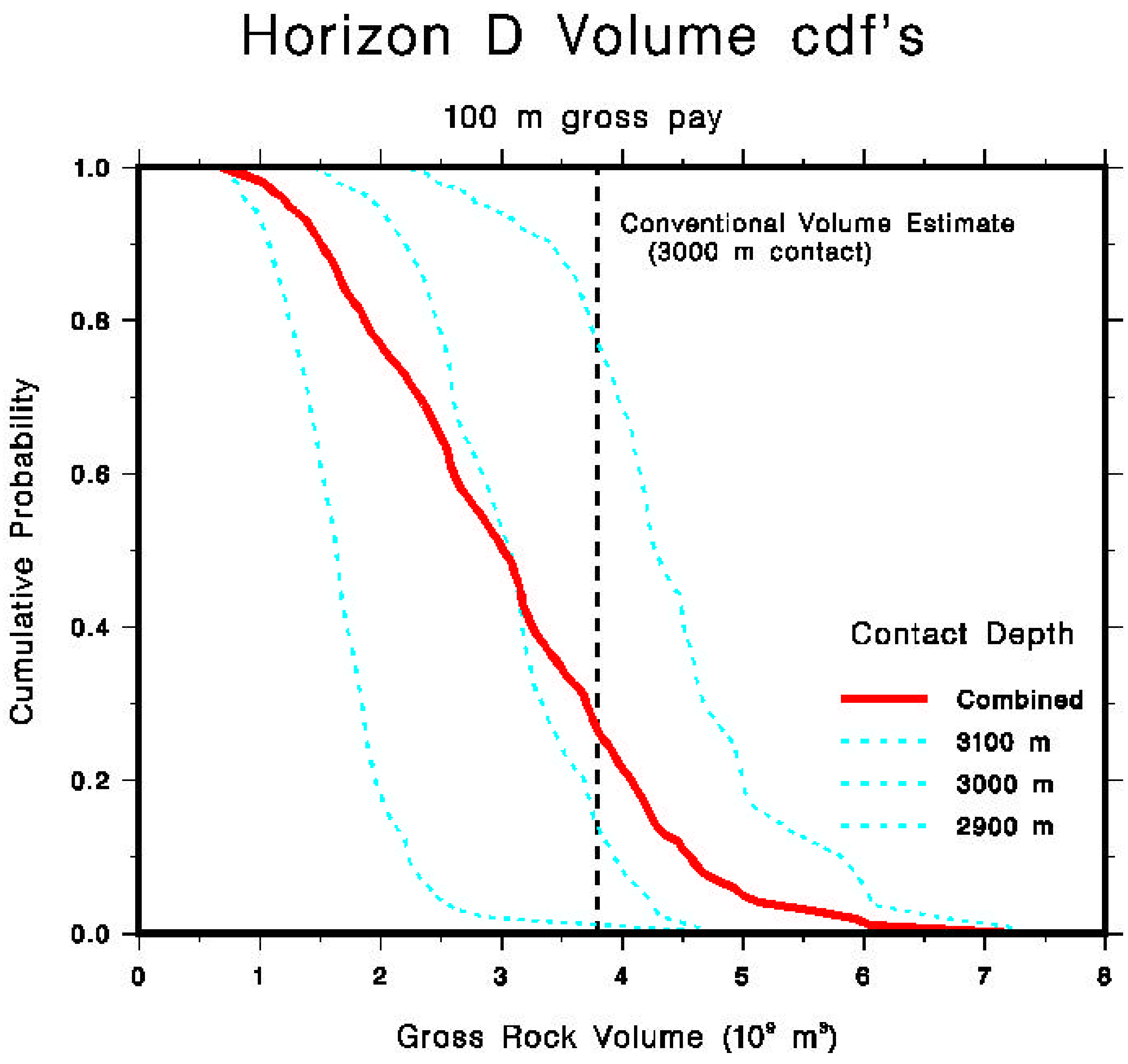
Horizon D Volume cdf's
100 m gross pay
Conventional Volume Estimate
(3000 m contact)
Contact Depth
Combined
3100 m
3000 m
2900 m
Cumulative Probability
Gross Rock Volume (10⁹ m³)
1.0
0.8
0.6
0.4
0.2
0.0
0
1
2
3
4
5
6
7
8